ARTICLES

Luminescence and Energy Transfer of $[Ru(bpy)_3]^{2+}$, $[Cr(ox)_3]^{3-}$, and $[Os(bpy)_3]^{2+}$ in Three-Dimensional Oxalato-Networks

Marianne E. von Arx, Emanuele Burattini, and Andreas Hauser*

Département de chimie physique, Université de Genève, 30, quai E.-Ansermet, 1211 Geneva 4, Switzerland

Liesbeth van Pieterson

Debye Research Institute, University Utrecht, P.O. Box 80000, 3508 TA Utrecht, Netherlands

René Pellaux and Silvio Decurtins

Departement für Chemie und Biochemie, Universität Bern, Freiestrasse 3, CH-3000 Bern 9, Switzerland

Received: September 21, 1999

Luminescence and energy transfer in $[Zn_{1-x}Ru_x(bpy)_3][NaAl_{1-y}Cr_y(ox)_3]$ ($x \approx 0.01$, $y = 0.006 - 0.22$; bpy = 2,2′-bipyridine, ox = $C_2O_4^{2-}$) and $[Zn_{1-x-y}Ru_xOs_y(bpy)_3][NaAl(ox)_3]$ ($x \approx 0.01$, $y = 0.012$) are presented and discussed. Surprisingly, the luminescence of the isolated luminophores $[Ru(bpy)_3]^{2+}$ and $[Os(bpy)_3]^{2+}$ in $[Zn(bpy)_3][NaAl(ox)_3]$ is hardly quenched at room temperature. Steady-state luminescence spectra and decay curves show that energy transfer occurs between $[Ru(bpy)_3]^{2+}$ and $[Cr(ox)_3]^{3-}$ and between $[Ru(bpy)_3]^{2+}$ and $[Os(bpy)_3]^{2+}$ in $[Zn_{1-x}Ru_x(bpy)_3][NaAl_{1-y}Cr_y(ox)_3]$ and $[Zn_{1-x-y}Ru_xOs_y(bpy)_3]$ $[NaAl(ox)_3]$, respectively. For a quantitative investigation of the energy transfer, a shell type model is developed, using a Monte Carlo procedure and the structural parameters of the systems. A good description of the experimental data is obtained assuming electric dipole−electric dipole interaction between donors and acceptors, with a critical distance R_c for $[Ru(bpy)_3]^{2+}$ to $[Cr(ox)_3]^{3-}$ energy transfer of 15 Å and for $[Ru(bpy)_3]^{2+}$ to $[Os(bpy)_3]^{2+}$ energy transfer of 33 Å. These values are in good agreement with those derived using the Förster−Dexter theory.

1. Introduction

The class of cubic, three-dimensional metal-tris-oxalate network structures with tris-bipyridine complexes as counter ions of general compositions $[M_a^{II}(bpy)_3][M_c^{I}M_b^{III}(ox)_3]$ and $[M_a^{III}(bpy)_3][M_c^{I}M_b^{III}(ox)_3]ClO_4$ (bpy = 2,2′-bipyridine, ox = $C_2O_4^{2-}$) first synthesized by Decurtins et al.[1] have interesting structural, magnetic, and photophysical properties.[2] Chemical variation and combination of metal ions of different valencies in the oxalate backbone as well as in the tris-bipyridine complexes offer unique opportunities for investigating a large variety of photophysical processes, from straight forward luminescence to light-induced electron transfer, and excitation energy transfer. A photosensitizer can be incorporated either into the oxalate backbone or the tris-bipyridine cation, in low concentration as dopant, at higher concentrations in mixed crystals, or fully concentrated in neat compounds.

Recently, we reported on energy transfer processes in neat $[Rh(bpy)_3][NaCr(ox)_3]ClO_4$[3] and in mixed crystals of composition $[Rh_{1-x}Cr_x(bpy)_3][NaAl_{1-y}Cr_y(ox)_3]ClO_4$,[4] respectively, using steady-state and time-resolved luminescence spectroscopy. For the former, we showed that the energy migration among $[Cr(ox)_3]^{3-}$ at 1.5 K is a truly resonant process, while at higher temperatures phonon-assisted energy transfer becomes important.[3] In the latter, we identified two different interaction mechanisms for the energy transfer from $[Cr(ox)_3]^{3-}$ to $[Cr(bpy)_3]^{3+}$.[3] A rapid, short-range process was attributed to superexchange coupling between $[Cr(ox)_3]^{3-}$ and $[Cr(bpy)_3]^{3+}$ via π-overlap of the oxalate and bipyridine ligands. At low $[Cr(bpy)_3]^{3+}$ concentrations, in addition, a much slower process was found, which was attributed to an electric dipole−electric dipole mechanism.

In the present paper we investigate the excitation energy transfer from $[Ru(bpy)_3]^{2+}$ as the initially excited donor to both $[Os(bpy)_3]^{2+}$ and $[Cr(ox)_3]^{3-}$ in the mixed crystal systems of compositions $[Zn_{1-x-y}Ru_xOs_y(bpy)_3][NaAl(ox)_3]$ and $[Zn_{1-x}Ru_x(bpy)_3][NaAl_{1-y}Cr_y(ox)_3]$, using steady state and time-resolved luminescence spectroscopy. Rather than use the model of Inokuti and Hirayama,[5] which assumes a continuous distribution of distances between donors and acceptors, we use the actual structural data of our compounds[1,6] in a shell type model,[7,8] which is more appropriate for crystalline systems, for a quantitative interpretation of the experimental data. The method is based on the determination of the statistical probability distribution of the occupancy by acceptor ions of a specific shell around a given donor using a Monte Carlo procedure. This occupancy distribution serves as basis for the calculation of the distribution of the energy transfer rate constants and, subsequently, the relative donor and acceptor luminescence intensities as well as the corresponding decay curves.

Of course, there have been previous studies on energy transfer

10.1021/jp993368v CCC: $19.00
Published on Web 01/19/2000

TABLE 1: Nominal and Effective Mole Fractions[a] for $[Cr(ox)_3]^{3-}$, $[Ru(bpy)_3]^{2+}$, $[Os(bpy)_3]^{2+}$, and $[Ru(bpy)_3]^{2+}$

$[Zn_{1-x}Ru_x(bpy)_3][NaAl_{1-y}Cr_y(ox)_3]$[b]			
$[Cr(ox)_3]^{3-}$ (mole fractions)		$[Ru(bpy)_3]^{2+}$ (mole fractions)	
nominal	effective	nominal	effective
0.01	0.006 ± 0.002	0.001	0.008 ± 0.003
0.05	0.036 ± 0.004	0.001	0.0065 ± 0.002
0.10	0.076 ± 0.01	0.001	0.007 ± 0.004
0.25	0.215 ± 0.02	0.001	0.01 ± 0.005

$[Zn_{1-x}Ru_xOs_ybpy)_3][NaAl(ox)_3]$[c]			
$[Os(bpy)_3]^{2+}$ (mole fractions)		$[Ru(bpy)_3]^{2+}$ (mole fractions)	
nominal	effective	nominal	effective
0.01	0.012 ± 0.003	0.001 (?)	0.019 ± 0.005

[a] Nominal mole fraction: as in solution. Effective mole fraction: from X-ray fluorescence. [b] Nominal and effective mole fractions for $[Os(bpy)_3]^{2+}$ and $[Ru(bpy)_3]^{2+}$ in $[Zn_{1-x}Ru_x(bpy)_3][NaAl_{1-y}Cr_y(ox)_3]$. [c] Nominal and effective mole fractions for $[Os(bpy)_3]^{2+}$ and $[Ru(bpy)_3]^{2+}$ in $[Zn_{1-x-y}Ru_xOs_y(bpy)_3][NaAl(ox)_3]$.

with the ubiquitous $[Ru(bpy)_3]^{2+}$ complex and its derivatives as photosensitiser and osmium(II)[9−15] and chromium(III)[16−18] complexes as acceptors. The key difference between these studies and our work is that whereas the former have been conducted on dinuclear species either in solution at room temperature or at 77 K in glassy matrices, we work with well-defined, crystalline materials at or near liquid helium temperatures.

2. Experimental Section

Preparation and Characterization of Samples. Polycrystalline samples of the mixed crystal series $[Ru_{1-x}Os_x(bpy)_3][NaAl_{1-y}Cr_y(ox)_3]$ and $[Ru(bpy)_3][NaAl_{1-x}Cr_x(ox)_3]$ (bpy = 2,2′-bipyridine and ox = oxalate) were prepared as described in refs 1 and 6. Basically the same method was applied to the preparation of $[Zn_{1-x}Ru_x(bpy)_3][NaAl_{1-y}Cr_y(ox)_3]$ and $[Zn_{1-x-y}Ru_xOs_ybpy)_3][NaAl(ox)_3]$. However, during the actual synthesis the reaction mixtures were kept at ∼0 °C using a bath with an ice−salt−water mixture, and a small amount of ethanol was added to the reaction mixture in order to prevent it from freezing. For the synthesis of mixed crystals of different concentrations, appropriate nominal mole fractions in aqueous solution of $K_3[Al(ox)_3]\cdot 3H_2O$ to $K_3[Cr(ox)_3]\cdot 3H_2O$ and $[Zn(bpy)_3]Cl_2\cdot 6H_2O$ to $[Ru(bpy)_3]Cl_2\cdot 6H_2O$ or $[Os(bpy)_3]Cl_2\cdot 6H_2O$ were used.

The crystal structures were checked by X-ray powder diffraction. All compounds crystallise in the cubic space group $P2_13$ (ref 1) with the $[M^{II}(bpy)_3]^{2+}$ and $[M^{III}(ox)_3]^{3-}$ units having C_3 site symmetry. The unit cell lengths are $a = 15.48$ Å for $[Zn(bpy)_3][NaAl(ox)_3]$, 15.37 Å for $[Ru(bpy)_3][NaAl(ox)_3]$, and 15.28 Å for $[Ru(bpy)_3][NaCr(ox)_3]$, and $Z = 4$.

The effective concentrations of Cr, Os, and Ru in the mixed crystals were determined by X-ray fluorescence. The results are summarized in Table 1 for the series $[Zn_{1-x}Ru_x(bpy)_3][NaAl_{1-y}Cr_y(ox)_3]$ and $[Zn_{1-x-y}Ru_xOs_ybpy)_3][NaAl(ox)_3]$, respectively. The effective Cr concentration was found to be consistently smaller than the nominal concentration as derived from the corresponding mole fraction in solution. The Ru concentration is roughly the same in all samples, but with 0.7 ± 0.2 mol % it is substantially higher than the nominal concentration of 0.1 mol %. Similarly, with 1.2 ± 0.3 mol %, the effective Os concentration is slightly higher than the 1% nominal concentration. Conversely, the concentration determination on $[Ru(bpy)_3][NaAl_{1-x}Cr_x(ox)_3]$ and $[Ru_{1-x}Os_x(bpy)_3][NaAl_{1-y}Cr_y(ox)_3]$ shows that in these systems the Cr concentration is slightly higher and the Os concentration slightly smaller than their respective nominal concentrations.

Spectroscopy. Luminescence spectra were obtained by exciting with an Ar^+/Kr^+ mixed gas ion laser (Spectra Physics Stabilite 2108) at 476 and 488 nm. Luminescence was dispersed by a 85 cm double monochromator (Spex 1404). A cooled GaAs photomultiplier tube (RCA-C31034) was used as detector, and the signal was processed by a photon counting system (StanfordResearch SR 400). All luminescence spectra are corrected for instrumental response.

Decay curves were acquired using two different excitation sources. For fast processes, the output of a pulsed and frequency doubled Nd:YAG laser (Quantel BrilliantB; FWHM pulse width ∼7 ns, 20 Hz repetition rate, $\lambda_{ex} = 532$ nm) was used. For slower time-resolved measurements, the output of the Ar^+/Kr^+ ion laser was passed through an acousto-optic modulator (Automates and Automatismes MT 0808) and modulation pulses between 1 and 10 μs were generated with a function generator (Stanford Research Systems DS 345). Decay curves were recorded with a multichannel scaler (Stanford Research SR 430) for low light levels and with a digital oscilloscope (Tektronix TDS 540B) for high light levels. The above mentioned cooled GaAs photomultiplier tube as well as a room temperature multialkaline PM tube (Hamamatsu H957-08) in conjunction with fast preamplifiers (LeCroy VV 100BTB) were used for light detection. The overall bandwidth of the detection systems was approximately 50 MHz.

Sample temperatures between 11 and 300 K were achieved in a He closed cycle cryostat with the sample sitting in an atmosphere of He-exchange gas (Oxford Instruments CCC1204). Temperatures between 1.5 and 20 K were achieved in a liquid He cryostat (Oxford Instruments Optistat Bath) and controlled by a PID temperature controller (Oxford Instruments ITC601). A Macintosh PC served to control instrumentation and gather data via a GPIB interface, using powerful software developed by Oetliker on the National Instruments LabView platform.[19]

3. Results

Upon excitation at 21000 cm^{-1}, which is into the ^{1}MLCT absorption band[20] of $[Ru(bpy)_3]^{2+}$ in $[Ru(bpy)_3][NaAl_{0.99}Cr_{0.01}(ox)_3]$, broad band luminescence below 18000 cm^{-1} is observed, which can be assigned to the $^3MLCT \rightarrow {}^1A_1$ transition[21] of $[Ru(bpy)_3]^{2+}$. The corresponding luminescence spectrum at $T = 10$ K is shown in Figure 1a. In addition, sharp line luminescence is observed between 13500 and 14400 cm^{-1}. These characteristically sharp lines are assigned to the $^2E \rightarrow {}^4A_2$ transition[22] of $[Cr(ox)_3]^{3-}$. In the inset to Figure 1a the zero-field split electronic origins with the two well-known R-lines are shown.

Excitation into the ^{1}MLCT absorption of $[Ru(bpy)_3]^{2+}$ in $[Ru_{0.99}Os_{0.01}(bpy)_3]$ $[NaAl(ox)_3]$ also results in the characteristic broad band luminescence of the $^3MLCT \rightarrow {}^1A_1$ transition of $[Ru(bpy)_3]^{2+}$. However, Figure 1b shows that, at $T = 10$ K, this luminescence is very weak compared to an additional somewhat structured broad band luminescence below 14700 cm^{-1}. This luminescence is characteristic for the $^3MLCT \rightarrow {}^1A_1$ transition of $[Os(bpy)_3]^{2+}$.

With mole fractions of only 1%, direct excitation of the chromophores $[Cr(ox)_3]^{3-}$ and $[Os(bpy)_3]^{2+}$ can be neglected in the above systems. Therefore, the luminescence which is observed in addition to the $[Ru(bpy)_3]^{2+}$ luminescence has to be due to energy transfer from $[Ru(bpy)_3]^{2+}$ as donor to $[Cr(ox)_3]^{3-}$ and $[Os(bpy)_3]^{2+}$ acting as acceptors. In the case of $[Os(bpy)_3]^{2+}$ as acceptor, the $[Ru(bpy)_3]^{2+}$ luminescence is much more strongly quenched than with $[Cr(ox)_3]^{3-}$ as acceptor.

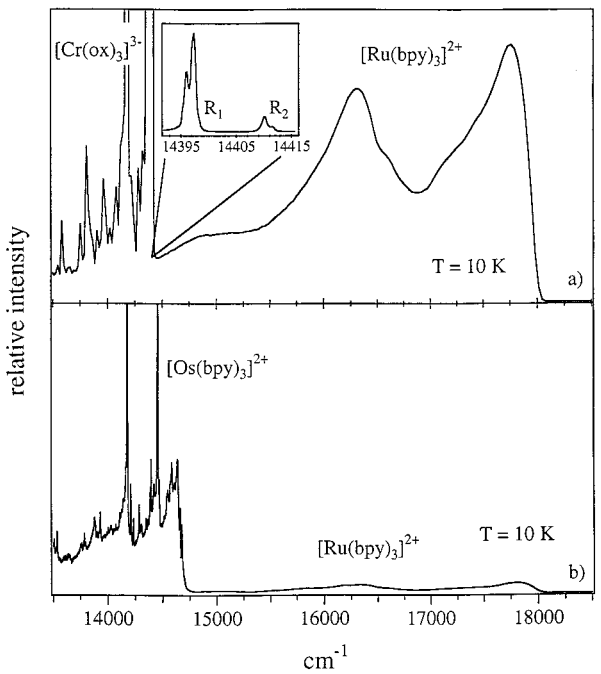

Figure 1. (a) Luminescence spectrum at 10 K of $[Ru(bpy)_3][Al_{0.99}Cr_{0.01}(ox)_3]$ upon excitation at 21000 cm^{-1}, that is into the ^{1}MLCT absorption band of $[Ru(bpy)_3]^{2+}$. Inset: Enlarged region of the *R* lines of the $[Cr(ox)_3]^{3-}$ luminescence. (b) Luminescence spectrum at 10 K of $[Ru_{0.99}Os_{0.01}(bpy)_3][NaAl(ox)_3]$ upon excitation at 21000 cm^{-1}.

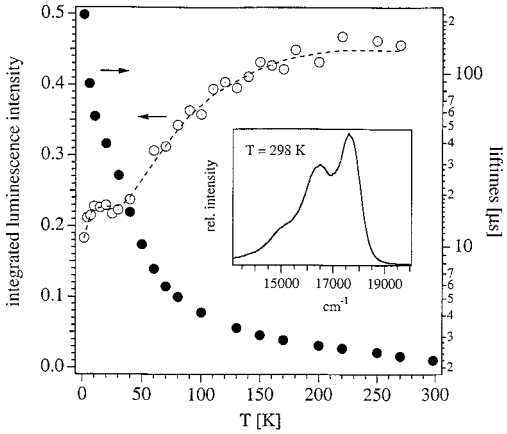

Figure 2. (⊙, left axis) Temperature dependence of the integrated $[Ru(bpy)_3]^{2+}$ luminescence intensity of $[Zn_{0.99}Ru_{0.01}(bpy)_3][NaAl(ox)_3]$ scaled to the luminescence quantum efficiency for $[Ru(bpy)_3]^{2+}$ at 10 K from ref 13. (− −) Guide for the eye of the resulting quantum efficiency η_{Ru} of the $[Ru(bpy)_3]^{2+}$ luminescence in $[Zn_{0.99}Ru_{0.01}(bpy)_3][NaAl(ox)_3]$. (●, right axis). Temperature dependence of the lifetime of the $[Ru(bpy)_3]^{2+}$ luminescence of $[Zn_{0.99}Ru_{0.01}(bpy)_3][NaAl(ox)_3]$. Inset: Luminescence spectrum of $[Zn_{0.99}Ru_{0.01}$ $(bpy)_3][NaAl(ox)_3]$ at 298 K.

Therefore, qualitatively the energy transfer to $[Os(bpy)_3]^{2+}$ can be said to be much more efficient than the one to $[Cr(ox)_3]^{3-}$.

Section 3 is structured as follows: As a preliminary, the luminescence behavior of the isolated luminophores $[Ru(bpy)_3]^{2+}$ and $[Os(bpy)_3]^{2+}$ in $[Zn_{1-x}M_x(bpy)_3]$ $[NaAl(ox)_3]$ ($M = Ru^{2+}, Os^{2+}; x \leq 0.01$) and of $[Cr(ox)_3]^{3-}$ in $[Zn(bpy)_3][NaA_{1-x}Cr_x(ox)_3]$ ($x \leq 0.01$) is presented in section 3.1. Sections 3.2 and 3.3 present the experimental results on the excitation energy transfer from $[Ru(bpy)_3]^{2+}$ to $[Cr(ox)_3]^{3-}$ in $[Zn_{1-x}Ru_x(bpy)_3][NaAl_{1-x}Cr_x(ox)_3]$ ($x \leq 0.01$, $y = 0.006, 0.036, 0.076, 0.22$), and from $[Ru(bpy)_3]^{2+}$ to $[Os(bpy)_3]^{2+}$ in $[Zn_{1-x-y}Ru_xOs_y(bpy)_3][NaAl(ox)_3]$ ($x \leq 0.01$, $y = 0.12$), respectively. Finally, section 3.4 presents the luminescence behavior of systems with higher concentrations of luminophores, for which additional donor−donor energy migration is to be expected.

3.1. Luminescence Behavior of the Isolated Luminophores. *$[Ru(bpy)_3]^{2+}$*. The inset of Figure 2 show the typical room temperature luminescence spectrum of $[Ru(bpy)_3]^{2+}$ in $[Zn_{1-x}Ru_x(bpy)_3][NaAl(ox)_3]$ ($x \approx 0.01$). Figure 2 itself shows the integrated luminescence intensity of $[Ru(bpy)_3]^{2+}$ for temperatures between 1.5 K and 270 K. The intensity increases with increasing temperatures all the way up to 270 K. There are two plateaux, one between 10 and 20 K, the other one asymptotically toward room temperature. The intensity at high temperature is approximately twice the intensity at 10 K.

In the diluted system, luminescence decay curves detected at 17986 cm^{-1} (556 nm) are single exponential. The corresponding lifetimes are also plotted as a function of temperature in Figure 2. The lifetime drops rapidly from ∼220 μs at 1.5 K to ∼60 μs at 10 K. There is a further substantial decrease to ∼4 μs between 10 and 100 K. At higher temperatures the lifetime decreases more gradually from about ∼4 μs at 100 K to ∼2.5 μs at 298 K. The decrease of the lifetime with increasing temperatures is in agreement with measurements on $[Ru(bpy)_3]^{2+}$ obtained in other matrices and the absolute values are on the same order of magnitude.[23,24] In particular, the low temperature behavior is in close agreement with literature values, only the room temperature value of ∼2.5 μs is substantially larger than in most other $[Ru(bpy)_3]^{2+}$ containing systems studied to date.

The temperature dependence of the integrated intensity, too, follows the known behavior up to 100 K. The observed increase has been attributed to three closely spaced luminescent states, having different temperature independent decay rates and different luminescence quantum efficiencies.[23] In Figure 2, the integrated luminescence has, in fact, been scaled to the luminescence quantum efficiency η_{Ru}, at 10 K of 0.225 as reported by Harrigan et al.[23] The broken line in Figure 2 can thus be regarded as the luminescence quantum efficiency of our system as a function of temperature. In the systems mentioned in refs 13 and 14, the luminescence intensity starts to decrease at temperatures above 100 K. This has been attributed to an additional, thermally activated, nonradiative process involving a close lying excited ligand-field state.[23] Surprisingly, in the present system this additional process is not effective up to 270 K. We assume that the quantum efficiency follows the intensity curve. Thus for our system η_{Ru} increases to a value of ∼0.45 at room temperature.

$[Os(bpy)_3]^{2+}$. The inset of Figure 3 shows the typical luminescence spectrum of $[Os(bpy)_3]^{2+}$ diluted in $[Zn_{1-x}Os_x(bpy)_3][NaAl(ox)_3]$ ($x \approx 0.01$) at 298 K. In Figure 3 itself, the integrated luminescence intensity of $[Os(bpy)_3]^{2+}$ is given for temperatures between 11 and 298 K. The intensity increases with increasing temperatures up to 250 K. Between 10 and 30 K the intensity is strongly temperature dependent. At higher temperatures there are two plateaux. For temperatures above 250 K the luminescence is slightly quenched. At 250 K, the luminescence intensity is about three times larger than at 10 K. As expected, luminescence decay curves detected at 14620 cm^{-1} (684 nm) show single exponential behavior. The luminescence lifetime is also plotted in Figure 3 as a function of temperature. The lifetime drops from ∼16 μs at 11 K to ∼250 ns at 298 K.

The above behavior of intensity and lifetime as a function of temperature is similar to that of the $[Ru(bpy)_3]^{2+}$ luminescence in the present oxalato-network. Up to 77 K it is also comparable to the behavior described in ref 25. In Figure 3, the integrated luminescence has been scaled to the luminescence quantum

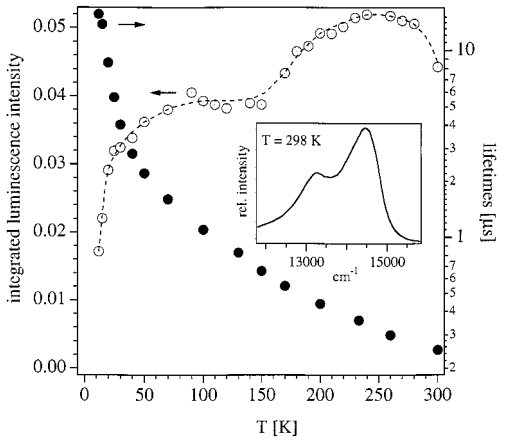

Figure 3. (⊙, left axis) Temperature dependence of the integrated $[Os(bpy)_3]^{2+}$ luminescence intensity of $[Zn_{0.99}Os_{0.01}(bpy)_3][NaAl(ox)_3]$ scaled to the luminescence quantum efficiency for $[Os(bpy)_3]^{2+}$ at 77 K from ref 15. (− −) Guide for the eye of the resulting quantum efficiency η_{Os} of the $[Os(bpy)_3]^{2+}$ luminescence in $[Zn_{0.99}Os_{0.01}(bpy)_3][NaAl(ox)_3]$. (●, right axis). Temperature dependence of the lifetime of the $[Os(bpy)_3]^{2+}$ luminescence of $[Zn_{0.99}Os_{0.01}(bpy)_3][NaAl(ox)_3]$. Inset: Luminescence spectrum of $[Zn_{0.99}Os_{0.01}(bpy)_3][NaAl(ox)_3]$ at 298 K.

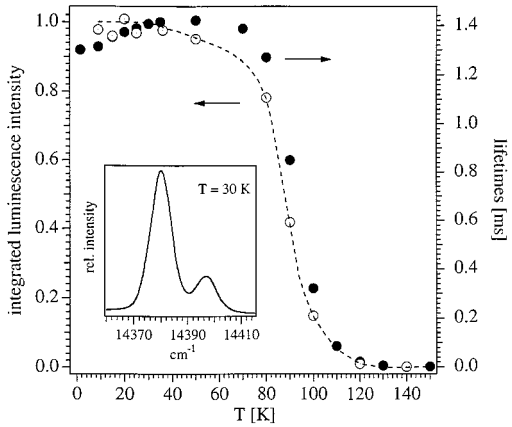

Figure 4. (⊙, left axis) Temperature dependence of the integrated $[Cr(ox)_3]^{3-}$ luminescence intensity of $[Zn(bpy)_3][NaAl_{0.995}Cr_{0.005}(ox)_3]$ scaled to 1 at 20 K. (− −) Guide for the eye of the quantum efficiency η_{Cr} of the $[Cr(ox)_3]^{3-}$ luminescence in $[Zn(bpy)_3][NaAl_{0.995}Cr_{0.005}(ox)_3]$. (●, right axis). Temperature dependence of the lifetime of the $[Cr(ox)_3]^{3-}$ luminescence of $[Zn(bpy)_3][NaAl_{0.995}Cr_{0.005}(ox)_3]$. Inset: Luminescence spectrum of $[Zn(bpy)_3][NaAl_{0.995}Cr_{0.005}(ox)_3]$ at 30 K.

efficiency η_{Os} at 77 K of 0.038 as reported by Lacky et al.[25] Note, that the quantum efficiency of the $[Os(bpy)_3]^{2+}$ luminescence, too, increases with increasing temperature up to nearly room temperature.

$[Cr(ox)_3]^{3-}$. Figure 4 shows the integrated luminescence intensity of $[Cr(ox)_3]^{3-}$ diluted in $[Zn(bpy)_3][NaAl_{1-x}Cr_x(ox)_3]$ ($x \approx 0.005$) at temperatures between 1.5 and 150 K. From the luminescence spectrum at 30 K in the inset of Figure 4, the energy difference between the two R-lines of the $^2E \rightarrow {}^4A_2$ transition is determined to be 17 cm^{-1}. From a Boltzmann analysis of the luminescence spectra at different temperatures, a ratio of the oscillator strengths of $f(R_1)/f(R_2) = 2$ is found. This ratio is in agreement with the ratio obtained from absorption spectra in related oxalato-network structures with $f(R_1) \approx 5.6 \times 10^{-7}$ and $f(R_2) \approx 2.8 \times 10^{-7}$.[3,6] The integrated luminescence intensity is roughly constant between 10 and 40 K. Above 40 K it starts to decrease, and at temperatures higher than 150 K the luminescence is completely quenched.

As expected, all decay curves show single exponential

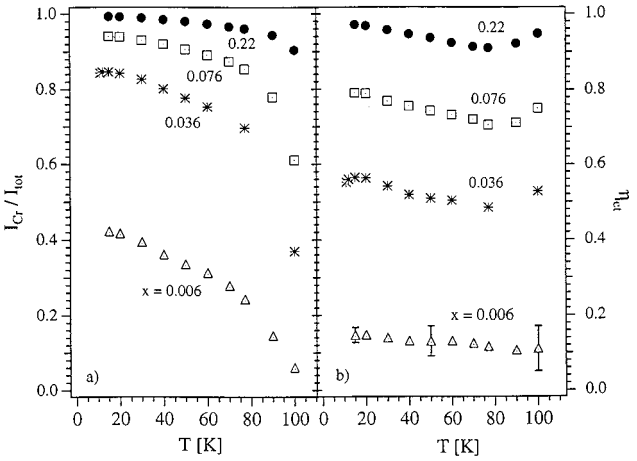

Figure 5. (a) Temperature dependence of the integrated $[Cr(ox)_3]^{3-}$ luminescence I_{Cr} normalized to the total luminescence intensity, $I_{tot} = I_{Cr} + I_{Ru}$, of $[Zn_{0.993}Ru_{0.007}(bpy)_3][NaAl_{1-x}Cr_x(ox)_3]$ with $x = 0.006$, 0.036, 0.076, and 0.22. (b) Quantum efficiency for $[Ru(bpy)_3]^{2+}$ to $[Cr(ox)_3]^{3-}$ energy transfer η_{et} derived from Figure 5a using eq 1 and η_{Ru} and η_{Cr} from Figures 2 and 4, respectively.

behavior. The corresponding lifetime as a function of temperature is included in Figure 4. At 1.5 K the lifetime is 1.3 ms. It increases slightly up to 50 K, then it starts to decrease. The initial increase is due to the Boltzmann equilibrium between the R-lines and their different oscillator strengths; the decrease above 50 K, which parallels the decrease of the integrated intensities, shows that at higher temperatures a thermally activated nonradiative processes sets in, completely quenching the luminescence above 150 K. With an oscillator strength of the R_1 line of 5.6×10^{-7}, a radiative lifetime at $T \rightarrow 0$ of ~2 ms can be estimated.[26] In view of the fact that the luminescence intensity below 40 K is constant, it seems fair to assume that the experimental lifetime of 1.3 ms at 10 K corresponds to the actual radiative lifetime, and that at low temperatures the luminescence quantum yield is close to unity. With this assumption, the luminescence quantum yield as a function of temperature follows the integrated intensity scaled to unity at $T \rightarrow 0$.

3.2. Energy Transfer from $[Ru(bpy)_3]^{2+}$ to $[Cr(ox)_3]^{3-}$. In $[Zn_{0.993}Ru_{0.007}(bpy)_3][NaAl_{1-x}Cr_x(ox)_3]$ with $x = 0.006$, 0.036, 0.076, and 0.22, direct excitation of $[Cr(ox)_3]^{3-}$ acceptors is negligible at the irradiation wavelength of $\lambda = 476$ nm (21000 cm^{-1}). Therefore the ratio of the integrated intensity of $[Ru(bpy)_3]^{2+}$ to $[Cr(ox)_3]^{3-}$ luminescence is a measure for the efficiency of energy transfer. Figure 5a shows the intensity of the $[Cr(ox)_3]^{3-}$ luminescence I_{Cr} normalized to the total luminescence intensity $I_{tot} = I_{Cr} + I_{Ru}$ for the above mentioned acceptor concentrations as a function of temperature from 11 to 100 K. For each concentration, the relative intensity decreases with increasing temperature. Using the data for intrinsic luminescence quantum yields as a function of temperature for the two luminophores, η_{Cr} and η_{Ru}, as given in section 3.1, it is straight forward to calculate the overall quantum yield of the $[Ru(bpy)_3]^{2+}$ to $[Cr(ox)_3]^{3-}$ energy transfer from the data of Figure 5a:

$$\eta_{Cr} = \frac{I_{Cr}/\eta_{Cr}}{I_{Cr}/\eta_{Cr} + I_{Ru}/\eta_{Ru}} \qquad (1)$$

Figure 5b shows that η_{et} is not very temperature dependent. It is on the order of 12% for $x = 0.006$ and rises to above 90% for $x = 0.22$.

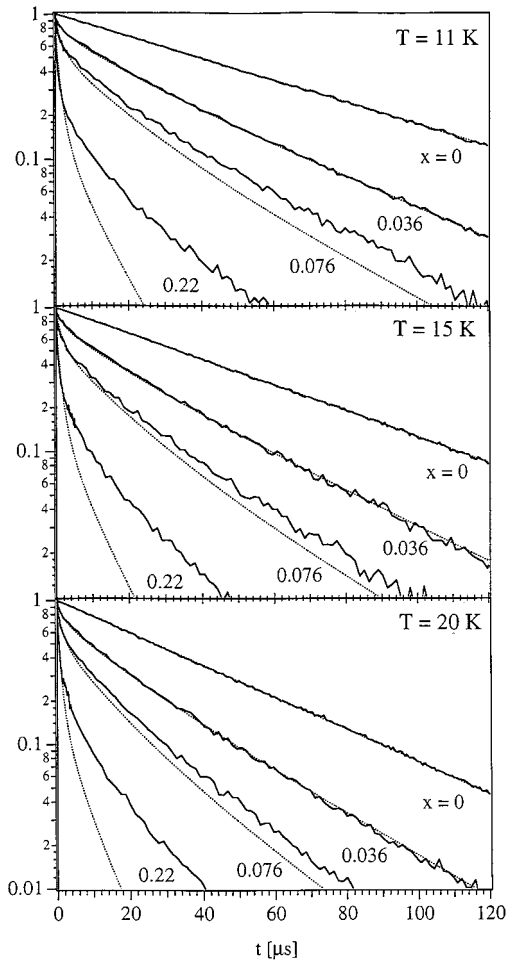

Figure 6. Experimental decay curves of the $[Ru(bpy)_3]^{2+}$ luminescence of $[Zn_{0.993}Ru_{0.007}(bpy)_3][NaAl_{1-x}Cr_x(ox)_3]$ with $x = 0$, 0.036, 0.076, and 0.22 upon excitation at 532 nm (18800 cm^{-1}) at temperatures $T = 11$, 15, and 20 K (−). Decay curves of the $[Ru(bpy)_3^{2+}$ luminescence calculated by the MC model using eq 6 with $R_c = 15$ Å for $x = 0.036$, 0.076, and 0.22 (···).

Figure 6 shows the decay curves of the $[Ru(bpy)_3]^{2+}$ luminescence for the $[Cr(ox)_3]^{3-}$ concentrations $x = 0.036$, 0.076, and 0.22 at $T = 11$, 15, and 20 K following pulsed excitation at 532 nm (18800 cm^{-1}), and in Figure 7 the decay curves of the $[Ru(bpy)_3]^{2+}$ luminescence for $x = 0.036$ and temperatures between 20 K and room temperature are given. In Figure 7, the time axis has been scaled to the intrinsic decay of the donor, $\tau_{int}(T)$. All the decay curves show nonexponential behavior, and the luminescence decays faster than the luminescence of isolated $[Ru(bpy)_3]^{2+}$ at the same temperature, which is included in Figures 6 and 7 as reference curve. Figure 6 shows that the higher the $[Cr(ox)_3]^{3-}$ concentration is, the faster the luminescence decays. A comparison of the decay curves in Figure 7 for temperatures 50−298 K, shows that with increasing temperature the energy transfer from $[Ru(bpy)_3]^{2+}$ to $[Cr(ox)_3]^{3-}$ becomes slightly more efficient.

3.3. Energy Transfer from $[Ru(bpy)_3]^{2+}$ to $[Os(bpy)_3]^{2+}$. The absorption bands of the two chromophores are very broad and quite similar in shape and in intensity. Therefore it is not possible to excite only $[Ru(bpy)_3]^{2+}$ in the dilute system $[Zn_{0.968}Ru_{0.02}Os_{0.012}(bpy)_3][NaAl(ox)_3]$. Thus in this system the ratio of the integrated luminescence of $[Os(bpy)_3]^{2+}$ and $[Ru(bpy)_3]^{2+}$ cannot be determined meaningfully. However, the decay curves of the $[Ru(bpy)_3]^{2+}$ luminescence can be recorded. Following the 7 ns pulse excitation at 532 nm (18800 cm^{-1}), the luminescence was detected at 600 nm (16670 cm^{-1}). Figure 8 shows the corresponding decay curves at 11, 15, and 20 K. They all present strongly non-exponential behavior, and the luminescence, too, decays much faster than the single exponential decay of isolated $[Ru(bpy)_3]^{2+}$ also displayed as reference curves in Figure 8.

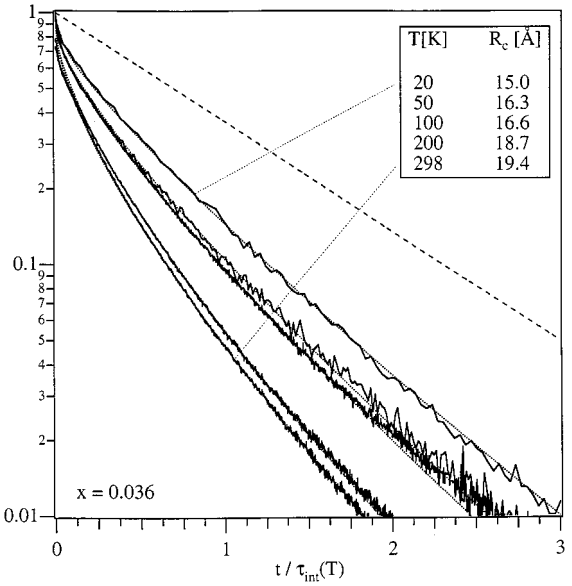

Figure 7. Temperature dependence of the experimental decay curves of the $[Ru(bpy)_3]^{2+}$ luminescence of $[Zn_{0.993}Ru_{0.007}(bpy)_3][NaAl_{1-x}Cr_x(ox)_3]$ with $x = 0.036$ upon excitation at 532 nm with the time axis scaled to $\tau_{int}(T)$ (−). Temperature dependence of the decay curves of the $[Ru(bpy)_3^{2+}$ luminescence derived from the MC model using eq 6 with values of R_c from 15 to 19.4 Å (···). The reference curve for $x = 0$ is single exponential, and in this representation it has a slope of unity (− −).

3.4. Energy Migration between $[Ru(bpy)_3]^{2+}$. Figure 9a shows the integrated steady state luminescence intensity of $[Ru(bpy)_3]^{2+}$ in (i) the diluted system $[Zn_{0.99}Ru_{0.01}(bpy)_3][NaAl(ox)_3]$ as already presented in section 3.1, in (ii) the mixed crystal series $[Zn_{1-x}Ru_x(bpy)_3][NaAl_{0.99}Cr_{0.01}(ox)_3]$ with $x \approx 0.03$, 0.3, 0.6, and 0.95, and in (iii) neat $[Ru(bpy)_3][NaAl(ox)_3]$ between 1.5 and 298 K. As discussed in section 3.1, the intensity for the diluted system increases with increasing temperature all the way from 1.5 to 300 K. In contrast, for neat $[Ru(bpy)_3][NaAl(ox)_3]$ the luminescence intensity increases only from 1.5 up to 6 K. At temperatures above ∼10 K, it starts to decrease strongly with increasing temperature, and at room temperature it is almost totally quenched. This, again, is in contrast to the mixed crystal systems for which the integrated luminescence intensity increases with temperature up to 80−100 K similar to the diluted system, and only starts to decrease at temperatures above ∼100 K, the quenching being stronger for higher values of x. The general behavior is thought to be due to energy migration between $[Ru(bpy)_3]^{2+}$ chromophores and efficient quenching by the 1 mol % $[Cr(ox)_3]^{3-}$ and killer traps. However, the initial increase of the luminescence intensity with increasing temperature for the mixed crystals, and even for $x = 0.95$, calls for a more sophisticated explanation (see below).

Figure 9b shows the dependence of the excited state lifetime of the $[Ru(bpy)_3]^{2+}$ in (i) of diluted $[Zn_{0.99}Ru_{0.01}(bpy)_3][NaAl(ox)_3]$ as already presented in section 3.1, in (ii) the mixed crystal series $[Zn_{1-x}Ru_x(bpy)_3][NaAl_{0.99}Cr_{0.0}(ox)_3]$ with $x \approx 0.3$, 0.6, and 0.95, and in (iii) neat $[Ru(bpy)_3][NaAl(ox)_3]$. Below ∼100 K the decay curves for all compounds show nearly single-exponential behavior. Except for the diluted system the decay curves recorded above ∼100 K show deviations from single-exponential behavior. The lifetimes plotted in Figure 9b are thus

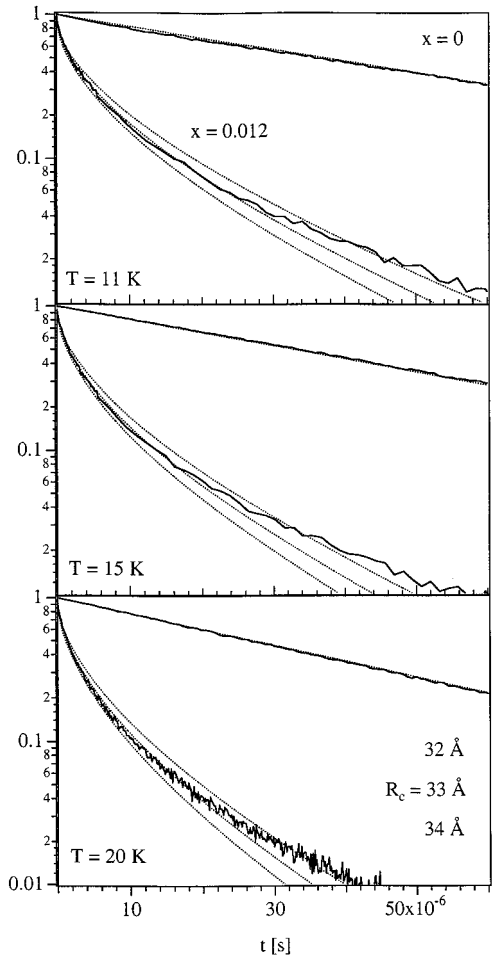

Figure 8. Experimental decay curves of the $[Ru(bpy)_3]^{2+}$ luminescence of $[Zn_{0.993-x}Ru_{0.007}Os_x(bpy)_3][NaAl(ox)_3]$ with $x = 0$ and 0.012 upon excitation at 532 nm (18800 cm^{-1}) at 11, 15, and 20 K (−). Decay curves of the $[Ru(bpy)_3]^{2+}$ luminescence derived from the MC model using eq 6 with values of $R_c = 32$, 33, and 34 Å for $x = 0.012$ (···). The reference curves for $x = 0$ are single exponential.

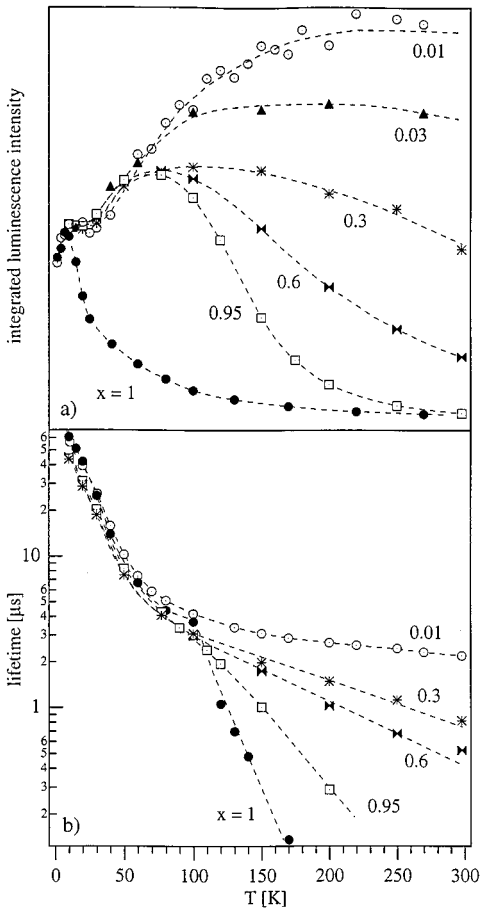

Figure 9. (⊙) (a) Temperature dependence of the integrated $[Ru(bpy)_3]^{2+}$ luminescence intensity of diluted $[Zn_{0.99}Ru_{0.01}(bpy)_3][NaAl(ox)_3]$, (▲) the mixed crystals series $[Zn_{1-x}Ru_x(bpy)_3][NaAl_{0.99}Cr_{0.01}(ox)_3]$ with $x \approx 0.03$, (∗) 0.3, (⋈), 0.6, and (⊡) 0.95, and neat $[Ru(bpy)_3][NaAl(ox)_3]$, scaled to 1 at 10 K (− − guide for the eye). (b) Temperature dependence of the corresponding excited state lifetimes (− − guide for the eye).

to be regarded as average values. The lifetimes decrease with increasing temperature for all systems. Up to ∼100 K the lifetimes for the diluted system, the neat compound and the mixed crystals are very similar. Above ∼100 K the lifetime of the diluted system decreases only slightly up to room temperature. In contrast, the lifetime of the neat $[Ru(bpy)_3][NaAl(ox)_3]$ starts to decrease strongly. Also in the mixed crystals, the lifetimes decreases more rapidly with increasing temperature than for the diluted system. The effect is larger for larger values of x.

4. The Model

4.1. Energy Transfer by a Dipole−Dipole Interaction-Mechanism. The energy transfer rate constant k_{et} from a donor to one single acceptor depends on the distance R_{da} between them. For the case of a dipole−dipole interaction mechanism it can be expressed as follows:[26]

$$k_{et}(R_{da}) = k_{int}\left(\frac{R_c}{R_{da}}\right)^6 \qquad (2)$$

where $k_{int} = 1/\tau_{int} = k_r + k_{nr}$ is the intrinsic decay rate constant of the donor without energy transfer, k_r being the radiative, and k_{nr} the nonradiative decay rate constant, respectively. R_c is the so-called critical distance for energy transfer, which is defined as the distance between the donor and an acceptor at which the energy transfer rate is equal to the intrinsic decay rate. Therefore, R_c is a measure for the strength of the dipole−dipole interaction. R_c can be calculated from the well known Förster−Dexter formula[27,28]

$$R_c^{\,6} = \text{const}\,\frac{Q_A\Omega_{DA}\,\eta_D}{n^4\tilde{\nu}_{DA}^4} \qquad (3)$$

Q_a is the integrated absorption cross section of the relevant acceptor transition, Ω_{da} is the spectral overlap integral of the normalized absorption and emission of acceptor and donor, respectively, η_d is the intrinsic luminescence quantum yield of the donor, $\tilde{\nu}_{da}$ is the energy at maximum spectral overlap, and n is the index of refraction. For Q_a and Ω_{da} in units of cm, $\tilde{\nu}_{da}$ in cm^{-1} and R_c in angstroms, const takes on a value of 1.62×10^{44} (see e.g., ref 26).

Let us first consider one excited ion as donor, which is surrounded, by other ions acting as acceptors in the energy transfer process. The latter may be collected into individual shells around the donor i. The shell labelled $i = 1$ corresponds to the shell of nearest neighbors, shell $i = 2$ to the one of next nearest neighbors, etc. The actual crystal structure defines the distances $R_{da}(i)$ and the number of lattice sites $N(i)$ at each distance. In order to describe the total energy transfer rate of one single donor, we must consider not only one acceptor but

all acceptors in its surroundings. Then the total energy transfer rate constant k_{et} for that donor is given as the sum of the rate constants $k_{et}(R_{da})$ for all acceptors:

$$k_{et} = k_{int}R_c^6\sum_i (R_{da}(i))^{-6}x(i) \qquad (4)$$

$R_{da}(i)$ is the distance between the donor and the acceptors in shell i, and $x(i)$ is the number of acceptors in this shell. In compounds with a low donor concentration on the one hand and an acceptor mole fraction equal to unity on the other, $x(i) = N(i)$, and k_{et} is the same for all donors. For mixed crystals with both acceptors as well as donors diluted in an inert host matrix this is no longer the case. $x(i)$ depends on the concentration of acceptors c_a, and the number of possible acceptor sites $N(i)$ in shell i.

Because the acceptors are randomly distributed, each donor has a different acceptor environment. Consequently, each donor has a different energy transfer rate constant. In the following we first present a method to calculate the resulting distribution of energy transfer rate constants, from which we then can calculate the ratio of the intensities of donor and acceptor luminescence as well as decay curves for the donor luminescence.

4.2. Distribution of Energy Transfer Rate Constants. In order to simulate the distribution of energy transfer rate constants for a system as described above, it is convenient to use Monte Carlo (MC) methods. A MC routine can quickly generate acceptor environments $x(i)$ for one particular donor and a given acceptor mole fraction, and given structural parameters. The corresponding values of k_{et} for $[Ru(bpy)_3]^{2+}$ to $[Cr(ox)_3]^{3-}$ and $[Ru(bpy)_3]^{2+}$ to $[Os(bpy)_3]^{2+}$ energy transfer follow from eq 4. In order to generate the distribution for a macroscopic system, the MC routine has to be repeated many times.

Energy Transfer from $[Ru(bpy)_3]^{2+}$ to $[Os(bpy)_3]^{2+}$. Figure 10a shows the distribution of energy transfer rate constants as $k_{et}/k_{int}R_c^6$ for energy transfer from $[Ru(bpy)_3]^{2+}$ to $[Os(bpy)_3]^{2+}$ for 1.2 mol % $[Os(bpy)_3]^{2+}$, using the structural parameters of Table 2 and considering values of R_{da} up to 47 Å (56 shells, 482 sites). The distribution is far from continuous due to the discrete values of distances between donors and acceptors. Because acceptors which are in the closest shell contribute most strongly, the three discrete values with their subdistributions can be explained by donors having 0, 1, or 2 acceptors in their nearest neighbor shell $i = 1$. At a mole fraction of 1.2%, the probability for having more than two sites in the nearest-neighbor shell occupied by acceptors is negligible. With a value of 14.55 Å, R_{da} of the second shell is substantially larger than the 9.4 Å of the first shell. Thus occupancy of the second and subsequent shells only results in a spread around the main peaks of the distribution. The inset shows a magnification of the subdistribution for which the nearest neighbor shell is occupied with $x(1) = 1$. It may be noted at this stage that the distribution of k_{et} expressed in units of $k_{int}R_c^6$ only depends upon the structural parameters and the concentration of acceptors. Thus the distribution of Figure 10a is valid for any donor acceptor pair with both donor and acceptor on tris-bpy sites and an acceptor mole fraction of 1.2%.

Energy Transfer from $[Ru(bpy)_3]^{2+}$ to $[Cr(ox)_3]^{3-}$. Figure 10b presents the distribution of energy transfer rate constants as $k_{et}/k_{int}R_c^6$ and a $[Cr(ox)_3]^{3-}$ concentration of 1.0 mol %, using the structural parameters of Table 2 and taking into account values of R_{da} up to 42 Å (106 shells, 333 sites). The structural data which determine the distribution of the energy transfer rate constants are somewhat different from those of the $[Ru(bpy)_3]^{2+}$−$[Os(bpy)_3]^{2+}$ system. In particular the value of R_{da} of the first shell is with 6.1 Å much smaller, and there is only one possible site to occupy. Due to this the resulting distribution in Figure 10b shows two regions, one at $k_{et}/k_{int}R_c^6$ around 20×10^{-6} Å^{-6} for shell 1 occupied, the other one between 0 and ~5 $\times 10^{-6}$ Å^{-6} for shell 1 not occupied. Note the large gap between the two regions! The two regions themselves are not continuous either and have subdistributions due to partial occupations of

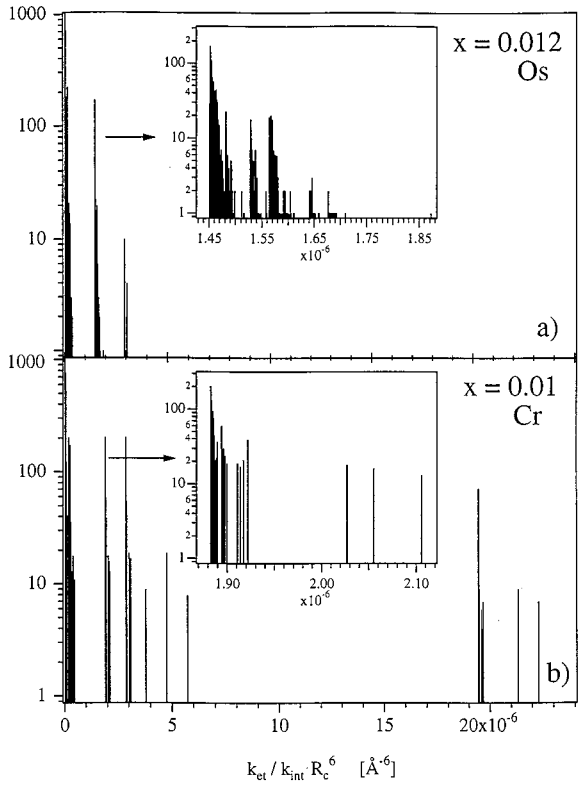

Figure 10. (a) Distribution of energy transfer rate constants k_{et} for the $[Ru(bpy)_3]^{2+}$ to $[Os(bpy)_3]^{2+}$ energy transfer in $[Zn_{0.993-x}Ru_{0.007}Os_x(bpy)_3][NaAl(ox)_3]$ with $x = 0.012$ in units of $k_{int}Rc^6$ as derived from a MC simulation considering 40000 donor environments. In the inset the subdistribution, for which the nearest neighbor shell is occupied by one donor, is shown on an expanded scale. (b) Distribution of energy transfer rate constants k_{et} for the $[Ru(bpy)_3]^{2+}$ to $[Cr(ox)_3]^{3-}$ energy transfer in $[Zn_{0.993}Ru_{0.007}(bpy)_3]$ $[NaAl_{1-x}Cr_x(ox)_3]$ with $x = 0.01$ in units of $k_{int}R_c^6$ as derived from a MC model considering 40000 donor environments. In the inset the subdistribution, for which the shells $i = 1$ and 2 are not occupied and shell 3 is singly occupied, is shown on an expanded scale.

TABLE 2: Distances $R_{da}(i)$ between the Ru and the Os or Cr, the Number of Possible Acceptor Sites N(i), and $k_{et}(R_{da})$ using eq 2 for shells $i = 1 - 11$[a]

	Ru−Os system			Ru−Cr system		
i	$R_{da}(i)$ [Å]	$N(i)$	$k_{et}(R_{da})$ $[k_{int}R_c^6]$	$R_{da}(i)$ [Å]	$N(i)$	$k_{et}(R_{da})$ $[k_{int}R_c^6]$
1	9.4	6	1.45×10^{-6}	6.1	1	1.94×10^{-5}
2	14.33	6	1.16×10^{-7}	8.4	3	2.84×10^{-6}
3	14.39	6	1.13×10^{-7}	9.0	3	1.88×10^{-6}
4	15.35	6	7.64×10^{-8}	12.84	3	2.24×10^{-7}
5	18.00	6	2.94×10^{-8}	13.4	3	1.73×10^{-7}
6	21.02	6	1.16×10^{-8}	13.8	3	1.45×10^{-7}
7	21.07	6	1.14×10^{-8}	17.15	6	3.93×10^{-8}
8	21.74	12	9.48×10^{-9}	17.5	3	3.48×10^{-8}
9	23.65	6	5.72×10^{-9}	17.8	3	3.14×10^{-8}
10	23.69	6	5.65×10^{-9}	18.1	3	2.84×10^{-8}
11	23.73	6	5.60×10^{-9}	19.6	3	1.76×10^{-8}

[a] The data were calculated from a common crystallographic program with the cubic space group $P2_13$, length of the unit cell $a = 15.37$ Å, and $Z = 4$.[8]

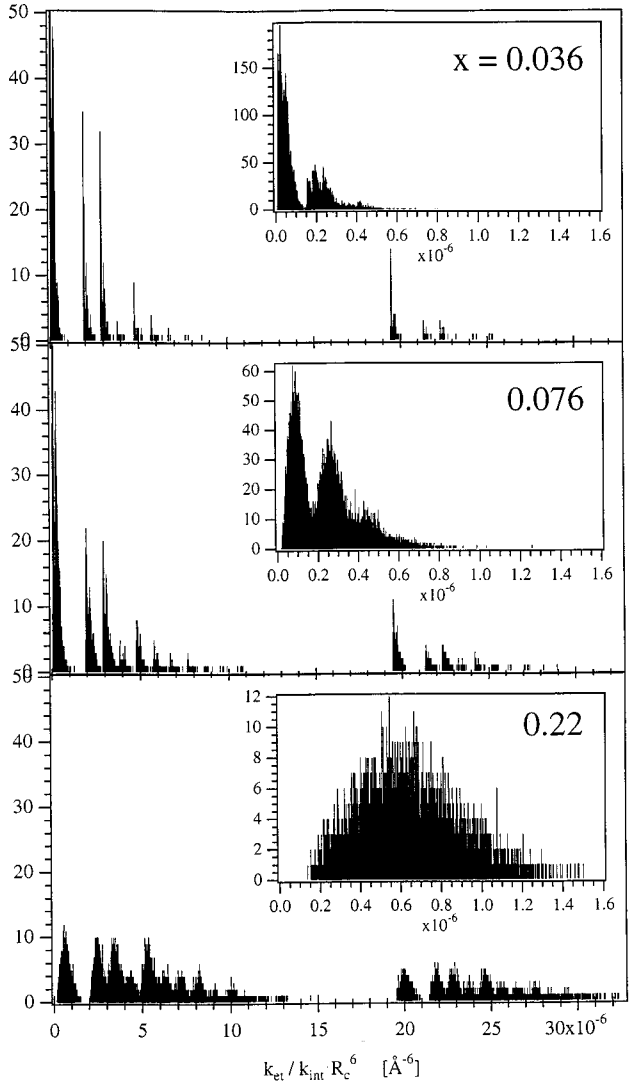

Figure 11. Distribution of energy transfer rate constants k_{et} for the $[Ru(bpy)_3]^{2+}$ to $[Cr(ox)_3]^{3-}$ energy transfer in $[Zn_{0.993}Ru_{0.007}(bpy)_3][NaAl_{1-x}Cr_x(ox)_3]$ with $x = 0.036$, 0.076, and 0.22 in units of $k_{int}R_c^6$ as derived from a MC model considering 40000 donor environments. In the inset the subdistribution, for which the shells $i = 1$, 2, and 3 are not occupied by acceptors, is shown on an expanded scale.

the shells 2 and 3 with $R_{da} = 8.4$ and 9.0 Å, respectively. In contrast to shell $i = 1$, shells 2 and 3 can be occupied by 3 acceptors. Thus they contribute to each region with several subdistributions. The inset shows the magnification of the region where shells 1 and 2 are not occupied and shell 3 is singly occupied.

Figure 11a−c show the distribution of energy transfer rate constants for the higher acceptor concentrations of 3.6, 7.7, and 22 mol %. Also in these distributions the two above mentioned characteristic regions with their subdistributions can be seen. At higher acceptor concentrations these subdistributions broaden, but nevertheless the subdistributions of the shells 2 and 3 can still be recognized within the two regions. In the insets the magnification of the regions where shells 1, 2, and 3 are not occupied is given. The inset of the 3.6 mol % system shows that there are donors having no acceptors within a reasonable distance, so that the donors will decay with approximately the intrinsic decay rate constant. In contrast, in the 22 mol % system, nearly all donors will decay faster than the intrinsic decay rate constant.

Decay Curves. Without any energy transfer the decay curve is given by its intrinsic decay rate constant k_{int} and is single exponential according to:

$$I(t) = I_0 e^{-k_{int}t} \tag{5}$$

$I(t)$ is the intensity of the donor luminescence at the time t and I_0 the intensity at $t = 0$.

As shown above, for a system doped with statistically distributed acceptors, the energy transfer rate constant k_{et} depends on the surroundings of the donor. Therefore, the decay curve of such a doped crystal will no longer be single exponential. Instead it is given by the sum of the exponential decay curves of each donor j over the total number of donors J according to

$$I(t) = \frac{I_0}{J}\sum_{j=1}^{J} e^{-[k_{int}+k_{et}(j)]t} \tag{6}$$

$I(t)$ can be calculated numerically from the distributions of k_{et} shown in Figures 10 and 11.

Steady State Luminescence.The intensities of the donor and acceptor luminescence in a steady state spectrum give information about the probability of the energy transfer. The probability P_{da} for an excited donor to transfer its energy to an acceptor instead of decaying intrinsically is given by

$$P_{da} = \frac{k_{et}}{k_{et} + k_{int}} \tag{7}$$

In the case of a distribution of the energy transfer rate constants, the over all quantum efficiency for energy transfer η_{et} is given by

$$\eta_{da} = \bar{P}_{da} = \frac{1}{J}\sum_{j=1}^{J} \frac{k_{et}(j)}{k_{et}(j) + k_{int}} \tag{8}$$

For a given R_c, η_{et} can be calculated numerically from the distribution of the k_{et} shown in Figures 10 and 11. Figure 12 shows the resulting η_{et} as a function of R_c for acceptor concentrations of 0.6, 3.6, 7.6, and 22 mol % for the case of $[Ru(bpy)_3]^{2+}$ to $[Cr(ox)_3]^{3-}$ energy transfer. η_{et} strongly depends on the acceptor concentration and on R_c. For high acceptor concentrations, η_{et} is very sensitive to R_c at small values of R_c, and saturates quickly with increasing R_c. For low acceptor concentrations, η_{et} is negligible at small values of R_c. It increases more slowly at intermediate values of R_c and saturates only at very large values of R_c. As a consequence, accurate experimental determination of η_{et} demands a range of appropriate acceptor concentrations. This range depends on R_c of the investigated energy transfer process. The higher R_c is, the smaller the concentration has to be.

5. Discussion

5.1. $[Ru(bpy)_3]^{2+}$ to $[Cr(ox)_3]^{3-}$ Energy Transfer. *Quantum Efficiency*. The experimentally determined quantum efficiency η_{et} for the $[Ru(bpy)_3]^{2+}$ to $[Cr(ox)_3]^{3-}$ energy transfer of Figure 5b can be readily used to estimate a value for R_c. The small apparent decrease of η_{et} with increasing temperature for higher concentration is probably not due to an actual decrease in η_{et}, but due to energy migration between $[Cr(ox)_3]^{3-}$ and concentration quenching.[3,4,29] The experimental values of η_{et} for the temperature range 10−20 K can therefore be regarded as typical

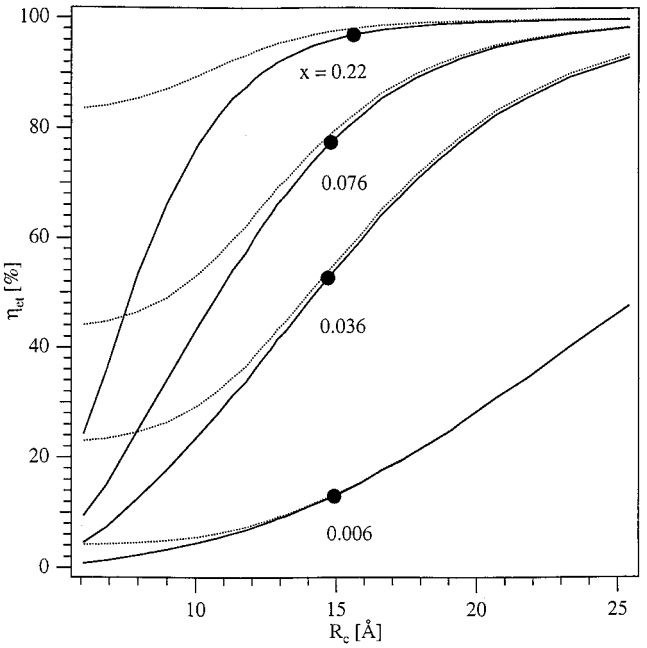

Figure 12. Quantum efficiencies for the $[Ru(bpy)_3]^{2+}$ to $[Cr(ox)_3]^{3-}$ energy transfer η_{et} in $[Zn_{0.993}Ru_{0.007}(bpy)_3][NaAl_{1-x}Cr_x(ox)_3]$ with $x =$ 0.006, 0.036, 0.076, and 0.22 for different values of R_c, calculated using eq 8 and the shell model for dipole−dipole interaction (−), and for dipole−dipole interaction with an additional very fast nearest neighbor energy transfer due to exchange interaction (···). Experimental values for (●) η_{et} from Figure 5b.

and have been entered into Figure 12. The resulting values of R_c for all concentrations fall within the narrow range of 15 ± 0.5 Å.

The above value for R_c can be compared to the one predicted based on eq 3. The relevant absorption of the acceptor is the $^4A_2 \rightarrow {}^4T_2$ transition of $[Cr(ox)_3]^{3-}$. The same absorption properties as in ref 6 are assumed for $[Cr(ox)_3]^{3-}$. With $\epsilon_{max} \approx$ 90 1 mol^{-1} cm^{-1} at $\tilde{\nu} = 17900$ cm^{-1} and $\Delta\tilde{\nu}_{1/2} \approx 2500$ cm^{-1}, Q_a takes on a value of $3.8 \times 10^{-21}\epsilon_{max}\Delta\tilde{\nu}_{1/2} = 8.6 \times 10^{-16}$ cm. The spectral overlap of the $^3MLCT \rightarrow {}^1A_1$ luminescence of $[Ru(bpy)_3]^{2+}$ with the $^4A_2 \rightarrow {}^4T_2$ absorption of $[Cr(ox)_3]^{3-}$ results in a value for Ω_{da} of $\sim 2 \times 10^{-4}$ cm. Together with the energy of maximum spectral overlap $\tilde{\nu}_{da} = 17700$ cm^{-1} and the quantum efficiency for the donor luminescence $\eta_d = 0.225$, eq 3 gives a value for R_c of 14.8 Å at 15 K. This is in excellent agreement with the one derived from the integrated luminescence intensities and the shell model.

Decay Curves. The distribution of energy transfer rate constants in mixed crystals is also responsible for the marked deviation of donor decay curves from single exponential behavior. In fact, it is straightforward to calculate such decay curves numerically for a given acceptor concentration using eq 6 and the distribution for $[Ru(bpy)_3]^{2+}$ to $[Cr(ox)_3]^{3-}$ transfer from section 4.2 (see Figure 11) together with the value of R_c of 15 Å as derived in the preceding paragraph, and the intrinsic decay rate constant of $[Ru(bpy)_3]^{2+}$ from section 3.1.

The calculated decay curves of the $[Ru(bpy)_3]^{2+}$ luminescence are included in Figure 6a−c for the $[Cr(ox)_3]^{3-}$ concentrations of 3.6, 7.6, and 22 mol % and for the same temperatures as the experimental curves, namely, for $T = 11$, 15, and 20 K. The calculated curves for 3.6 mol % $[Cr(ox)_3]^{3-}$ are in excellent agreement with the experimental data, and considering the fact that there is no actual curve fitting involved at this stage, the curves calculated for 7.6 mol % $[Cr(ox)_3]^{3-}$, too, are in acceptable agreement with the experimental curves. The initial, fast decay is due to donors having acceptors within their first three shells, and the somewhat slower part at intermediate times is due to donors with no acceptors within the first three shells but with acceptors still reasonably close to the donor for nonnegligible energy transfer. For the 3.6 mol % $[Cr(ox)_3]^{3-}$ sample there is a substantial number of donors with no acceptors within a reasonable distance. They, of course, decay with the intrinsic donor decay rate, and thus for long times, the decay curves of the donor luminescence have the same slopes in the logarithmic plots as the intrinsic decay curves.

As mentioned above, the agreement between calculated and experimental curves for the 7.6 mol % $[Cr(ox)_3]^{3-}$ sample is fair, particularly at short times. However, there are characteristic deviations. The calculated curves at longer times predict a faster decay of the donor luminescence than is actually observed. This effect becomes even more pronounced at the higher acceptor concentration of 22 mol % $[Cr(ox)_3]^{3-}$. There could be several reasons for this. Firstly, it cannot be excluded that in the polycrystalline samples the $[Cr(ox)_3]^{3-}$ chromophores are inhomogeneously distributed, either as a result of clustering within each crystallite or because of concentration gradients due to unfavourable distribution coefficients during crystal growth. A more likely explanation is provided in the form of a shielding effect as observed by Vasquez and Flint[7] in elpasolite crystals. This implies that at longer distances the dipole−dipole interaction is effectively shielded by the dielectric nature of the material. Thus the transfer at longer range is hindered to some extent, resulting in a slower decay of the donor luminescence than expected. According to Vasquez and Flint this shielding effect becomes more pronounced for higher acceptor concentrations. A third reason could be that the intrinsic decay of the $[Ru(bpy)_3]^{2+}$ luminescence in the mixed crystals containing $[Cr(ox)_3]^{3-}$ is not quite the same as in the diluted $[Zn_{1-x}Ru_x(bpy)_3][NaAl(ox)_3]$ with $x \approx 0.01$. Namely, the introduction of $[Cr(ox)_3]^{3-}$ may lead to local distortions, and thus the energy separations of the three luminescent states of $[Ru(bpy)_3]^{2+}$ may vary as a function of the $[Cr(ox)_3]^{3-}$ concentration.

Temperature Dependence. According to eq 3, the critical distance R_c depends on the integrated absorption cross section Q_a of the acceptor transition, the spectral overlap integral Ω_{da}, the resonance energy $\tilde{\nu}_{da}$, and on the luminescence quantum efficiency yield η_d of the donor. Whereas the temperature dependencies of Q_a, Ω_{da}, and $\tilde{\nu}_{da}$ are small for our case, η_d increases from ∼0.225 at 10 K to ∼0.37 at 100 K and to ∼0.45 at 298 K. Therefore R_c is expected to increase somewhat with increasing temperature.

Figure 7 shows that indeed the $[Ru(bpy)_3]^{2+}$ to $[Cr(ox)_3]^{3-}$ energy transfer does become slightly more efficient with increasing temperature in the sample with 3.6 mol % $[Cr(ox)_3]^{3-}$. Least-squares fits to the experimental curves were performed with R_c as the only variable parameter and using the distribution of rate constants of section 4.2 and the intrinsic decay rate constants of the $[Ru(bpy)_3]^{2+}$ luminescence from section 3.1. The one parameter fits are excellent for all experimental curves. Thus according to the decay curves of Figure 7, R_c increases from 15 Å at 20 K to 16.6 Å at 100 K and 19.4 Å at 298 K. These values have to be compared to the values of R_c calculated according to eq 3 and using the above values for η_d at 20, 100, and 298 K. The resulting calculated values of 14.8 Å and 16.1 Å for $T = 20$ and 100 K, respectively, are in good agreement with the fit values at these temperatures. The calculated high temperature value of 16.9 Å, however, is considerably smaller than the fit value of 19.4 Å at 298 K. This is in all probability due to the fact that the high temperature value of k_{int} is rather

sample dependent and may also be influenced by the incorporation of $[Cr(ox)_3]^{3-}$. In principle the quantum efficiency for the energy transfer η_{et} as a function of temperature shown in Figure 5b should also reflect the increase in R_c with increasing temperature. For the 0.6 mol % $[Cr(ox)_3]^{3-}$ it should, for instance, increase from ~13 to ~16% between 10 and 50 K and to ~17.5 % at 100 K. The accuracy of the experimental determination of η_{et} is not good enough to verify this prediction. If anything, experimentally η_{et} seems to decrease slightly with increasing temperature. However, this apparent decrease is not statistically significant and is probably due to the inaccuracies in the determination of the luminescence quantum efficiency of $[Cr(ox)_3]^{3-}$ at temperatures above ~50 K.

5.2. $[Ru(bpy)_3]^{2+}$ to $[Os(bpy)_3]^{2+}$ Energy Transfer. For the $[Ru(bpy)_3]^{2+}-[Os(bpy)_3]^{2+}$ system there is no relative intensity information available for an independent determination of R_c. Our only source of information are the decay curves of the donor luminescence shown in Figure 8. Included in Figure 8 are calculated decay curves of the donor luminescence using the distribution of energy transfer rate constants of section 4.2 (see Figure 10a) and the intrinsic decay rate constants at 11, 15, and 20 K from section 3.1. Model curves were calculated with values for R_c of 32, 33, and 34 Å. Although they do not give perfect fits, the curves with $R_c = 33$ Å are in fair agreement with the experimental curves.

The above value for R_c of 33 Å has to be compared to the one predicted based on eq 3. The absorption properties for the acceptor $[Os(bpy)_3]^{2+}$ can be estimated from the absorption spectrum of $[Os(bpy)_3]Cl_2$ in H_2O. From the relevant $^1A_1 \rightarrow {}^3$MLCT transition with $\epsilon \approx 3000$ 1 mol^{-1} cm^{-1} and $\Delta\tilde{\nu}_{1/2} \approx 4000$ cm^{-1}, the integrated absorption cross section Q_a takes on a value of 4.6×10^{-14} cm. The spectral overlap of the ^{3}MLCT $\rightarrow {}^1A_1$ luminescence of $[Ru(bpy)_3]^{2+}$ as donor and the absorption transition of the acceptor results in $\Omega_{da} = 3 \times 10^{-4}$ cm. Together with the energy $\tilde{\nu}_{da} = 16500$ cm^{-1} and the quantum efficiency for the donor $\eta_d = 0.225$ at 11 − 20 K, eq 3 gives $R_c \approx 32$ Å. This value is in an excellent agreement with the R_c derived from the decay curves using the shell model.

5.3. Energy Migration between $[Ru(bpy)_3]^{2+}$. There is a large contrast between the temperature dependence of the integrated luminescence intensity of isolated and concentrated $[Ru(bpy)_3]^{2+}$ in $[Zn_{0.99}Ru_{0.01}(bpy)_3][NaAl(ox)_3]$ and $[Ru(bpy)_3][NaAl(ox)_3]$, respectively (see Figure 9a). For the concentrated system, at temperatures above ~10 K energy migration between $[Ru(bpy)_3]^{2+}$ takes place and the intensity is quenched by energy transfer to killer traps, as for instance $[Fe(bpy)_3]^{2+}$. Such concentration quenching is typical for neat systems[30] and is usually very temperature dependent.

As stated above,[26−28] resonant energy transfer depends upon the spectral overlap between absorption and emission of acceptor and donor, respectively. For resonant energy transfer between like chromophores, this spectral overlap is restricted to the origin region. For systems with large Stokes shifts, the spectral overlap is inherently quite small even in an ideal crystal. In real systems, the homogeneous linewidths are usually substantially smaller than the inhomogeneous broadening, and thus the effective concentration of resonant molecules of the same species is greatly reduced. Therefore, resonant energy transfer between like chromophores is the exception[3] rather than the rule. More often, energy transfer between like chromophores is a temperature dependent phonon-assisted process.[26] Observed excited state lifetimes and luminescence intensities of the chromophores in highly concentrated systems depend strongly upon the width of the inhomogeneous distribution. For thermal energies k_BT larger than the width of the inhomogeneous distribution the energy travels freely within the crystal. Chances are that it will be taken up by a dopant center or a killer trap before luminescence occurs. As a result, the donor luminescence is strongly quenched and the average lifetime of the excited state is considerably reduced. If k_BT is much smaller than the inhomogeneous width, then the energy can only travel energetically down-hill within the inhomogeneous distribution. On its way it can either be annihilated by a dopant center or a killer trap, in which case it is lost. The energy which is not lost, ends up in a shallow trap, that is a donor chromophore at the low-energy side of the inhomogeneous distribution, where it remains trapped. As a result, the donor luminescence is quenched, but the observed luminescence decay corresponds to the lifetime of isolated donor chromophores. Finally, at very low temperatures, the phonon-assisted process is frozen in, the luminescence is not quenched and the lifetime, too, is equal to the one of the isolated donor.

On the basis of the above, the experimental results of Figure 9a and b can be easily rationalized: The inhomogeneous distribution of the excited state energies of $[Ru(bpy)_3]^{2+}$ in $[Ru(bpy)_3][NaAl(ox)_3]$ must be much narrower than that in $[Zn_{1-x}Ru_x(bpy)_3]$ $[NaAl(ox)_3]$ mixed crystals. Although the concentration of the $x = 0.95$ system is not significantly lower than that of the $x = 1$ system, energy migration does not take place up to ~80 K in the former system. Due to the broad inhomogeneous distribution the concentration of the shallow traps is very high so that the energy is efficiently trapped below 80 K. At temperatures above ~100 K efficient thermal detrapping occurs, resulting in a drop in the integrated luminescence intensity. The time-resolved experiments in Figure 9b show that also the luminescence of $[Ru(bpy)_3]^{2+}$ in $[Ru(bpy)_3][NaAl(ox)_3]$ below 100 K is due to shallow trap luminescence and at $T \approx$ 100 K thermal detrapping starts. Similarly, this detrapping above 100 K can also be seen in the $x = 0.6$ and 0.3 systems. Due to smaller $[Ru(bpy)_3]^{2+}$ concentrations the resulting migration into killer traps is less efficient, and consequently, the luminescence is less quenched.

6. Final Remarks

It is surprising and interesting that the luminescence of the isolated luminophores $[Ru(bpy)_3]^{2+}$ and $[Os(bpy)_3]^{2+}$ in $[Zn(bpy)_3][NaAl(ox)_3]$ is not or only slightly quenched at room temperature. A similar effect has been observed for $[Ru(bpy)_3]^{2+}$ confined to the cavities of Zeolites,[31,32] but in the present system the effect is even more pronounced. In a simple minded picture, the tight fit of the $[Ru(bpy)_3]^{2+}$ complex in both the Zeolite cavities as well as is in our network structures seems to destabilize the d−d quencher state with its substantially larger metal−ligand bond length via an internal pressure.

In our oxalate network systems, the $[Ru(bpy)_3]^{2+}$ to $[Os(bpy)_3]^{2+}$ energy transfer is dominated by an electric dipole−dipole mechanism. This contrasts sharply to the exchange mechanism postulated for the very efficient energy transfer in di- and polynuclear complexes with rigid bridging ligands having conjugated π-systems discussed in refs 12−15. On the other hand, it is in agreement with the work of Furue et al.[9] and Vögtle and DeCola et al.[10,11] who conclude that, for rigid and saturated bridging ligands, the much less efficient excitation energy transfer from $[Ru(bpy)_3]^{2+}$ to $[Os(bpy)_3]^{2+}$ proceeds to a large extent via an electric dipole−dipole mechanism, the rational being that through space exchange interaction is rather weak. Similarly, in the oxalate networks, an exchange pathway is implausible for the $[Ru(bpy)_3]^{2+}-[Os(bpy)_3]^{2+}$ system,

because the $[M^{II}(bpy)_3]^{2+}$ units are separated by at least 9.4 Å and they have neither direct bridging ligands nor is there any obvious π-overlap between ligand spheres. However, our value for the critical donor-acceptor separation R_c of 33 Å is substantially larger than the values between $\sim$10 Å[12−15] and 20 Å[9−11] estimated for the systems discussed in the above references, and thus our energy transfer efficiencies are on the same order of magnitude as those for the exchange coupled systems. This is basically due to the one to two orders of magnitude larger intrinsic luminescence quantum yield of $[Ru(bpy)_3]^{2+}$ embedded in the oxalate networks as compared to complexes in solution.

In the $[Ru(bpy)_3]^{2+}-[Cr(ox)_3]^{3-}$ donor−acceptor system, the situation looks quite similar to the one in $[Rh_{1-x}Cr_x(bpy)_3][NaAl_{1-y}Cr_y(ox)_3]ClO_4$, for which two different interaction mechanisms were identified for the $[Cr(ox)_3]^{3-}$ to $[Cr(bpy)_3]^{3+}$ energy transfer:[4] namely, the dipole−dipole mechanism with $R_c = 10.6$ Å and a super exchange mechanism due to a nearest neighbor interaction originating from π-overlap of the oxalate and bipyridine ligands. The ligands of the acceptor shells 1 and 2 have, in fact, very good π-overlap with the donor ligands, the ligand plane separation being only 3.7 Å, and also those in shell 3 still have nonnegligible overlap. $[Ru(bpy)_3]^{2+}$ to $[Cr(ox)_3]^{3-}$ energy transfer due to such an exchange mechanism would thus only affect donors having acceptors in the first three shells. With the MC shell model this can be taken into account. The dotted lines in Figure 12 represent η_{et} for the case that the exchange mechanism is so efficient, and that donors having an acceptor in the first three shells transfer their energy with a limiting probability of 100%. In addition to this exchange mechanism, the remaining shells contribute to η_{et} with a dipole−dipole interaction. The comparison with the η_{et} due to solely dipole−dipole interaction shows that for $R_c > \sim$14 Å the energy transfer quantum efficiency η_{et} is about the same with or without exchange mechanism. Therefore for the present system with $R_c = 15$ Å, the steady-state luminescence spectra give in principle no information as to the magnitude of a possible exchange interaction. However, in the decay curves an increase of the energy transfer rate constants of donors having acceptors in the first three shells would be expected due to such an exchange interaction. As a result, the decay curves in Figure 6 would decay much faster shortly after the pulse than the predicted curves assuming only dipole−dipole interaction. In the experimental curves no such initial acceleration is observed. Therefore, we conclude that the exchange mechanism is negligible and the dipole−dipole interaction mechanism is dominant.

With a critical distance of $R_c = 33$ Å, the energy transfer from $[Ru(bpy)_3]^{2+}$ to $[Os(bpy)_3]^{2+}$ is much more efficient than the energy transfer from $[Ru(bpy)_3]^{2+}$ to $[Cr(ox)_3]^{3-}$, for which $R_c = 15$ Å. According to eq 3, it is the 2 orders of magnitude larger absorption cross section of the $[Os(bpy)_3]^{2+}$ acceptor transition as compared to the one of the $[Cr(ox)_3]^{3-}$ transition which is responsible for this, the spectral overlap integrals being very close to each other.

The rigorous analysis of the energy transfer processes from $[Ru(bpy)_3]^{2+}$ to $[Os(bpy)_3]^{2+}$ and $[Cr(ox)_3]^{3-}$ has been possible due to the very special molecular architecture of our metal-trisoxalate network structures. Together with our previous studies[3,4] we have now demonstrated the versatility of these systems for quantitative energy transfer studies, resulting in unambiguous conclusions with regard to interaction mechanisms and to the nature of the various processes.

Acknowledgment. We thank Nahid Amstutz of the Université de Genève for the preparation of samples and Beatrice Frei of the Universität Bern for concentration measurements. This work was financially supported by the Swiss National Science Foundation. Preliminary data were recorded at the Universität Bern, and we thank H.U. Güdel for the use of equipment.

References and Notes

(1) Decurtins, S.; Schmalle, H. W.; Schneuwly, P.; Ensling, J.; Gütlich, P. *J. Am. Chem. Soc.* **1994**, *116*, 9521.
(2) Decurtins, S.; Pellaux, R.; Hauser, A.; von Arx, M. E. 484, In *Magnetism: A Supramolecular Function*; Kahn, O., Ed.; NATO ASI Series C; Kluwer Academic Publishers: Norwell, MA, 1996; p 487−508.
(3) (a) von Arx, M. E.; Hauser, A.; Riesen, H.; Pellaux, R.; Decurtins, S. *Phys. Rev. B* **1996**, *54*, 15800. (b) Hauser, A.; Riesen, H.; Pellaux, R.; Decurtins, S. *Chem. Phys. Lett.* **1996**, *261*, 313.
(4) Langford, V. S.; von Arx, M. E.; Hauser, A. **1999**, *J. Phys. Chem. A* **1999**. In press.
(5) Inokuti, M.; Hirayama, F. *J. Chem. Phys.* **1965**, *43*, 1978.
(6) Decurtins, S.; Schmalle, H. W.; Pellaux, R.; Schneuwly, P.; Hauser, A. *Inorg. Chem.* **1996**, *35*, 1451.
(7) Vasquez, S. O.; Flint, C. D. *Chem. Phys. Lett.* **1995**, *238*, 378.
(8) (a) Dornauf, H.; Heber, J. *J. Lum.* **1980**, *22*, 1. (b) Heber, J.; Dornauf, H.; Siebold, H. *J. Lum.* **1981**, *22*, 297. (c) Heber, J.; Dornauf, H.; Siebold, H. *J. Lumin.* **1981**, *24/5*, 735.
(9) Furue, M.; Yoshidzumi, T.; Kinoshita, s.; Kushida, T.; Nozakura, S.; Kamachi, M. *Bull. Chem. Soc. Jpn.* **1991**, *64*, 1632.
(10) Vögtle, F.; Frank, M.; Nieger, M.; Belser, P.; von Zelewski, A.; Balzani, V.; Barigelletti, F.; DeCola, L.; Flamigni, L. *Angew. Chem.* **1993**, *105*, 1706.
(11) DeCola, L.; Balzani, V; Barigelletti, F, Flamigni, L.; Belser, P.; von Zelewski, A.; Frank, M.; Vögtle, F. *Inorg. Chem.* **1993**, *32*, 5228.
(12) Belser, P.; von Zelewski, A.; Frank, M.; Seel, C.; Vögtle, F.; DeCola, L.; Barigelletti, F.; Balzani, V. *J. Am. Chem. Soc.* **1993**, *115*, 4076.
(13) Juris, A.; Balzani, V.; Campagna, S; Denti, G., Serroni, S.; Frei, G.; Güdel, H. U. *Inorg. Chem.* **1994**, *33*, 1491.
(14) Barigelletti, F.; Flamigni, L.; Balzani, V.; Collin, J.-P.; Sauvage, J.-P.; Sour, A.; Constable, E. C.; Cargill Thompson, A. M. W. *Coord. Chem. Rev.* **1994**, *132*, 209.
(15) Schlicke, B.; Belser, P.; DeCola, L.; Sabbioni, E.; Balzani, V. *J. Am. Chem. Soc.* **1999**, *121*, 4207.
(16) Scandola, F.; Bignozzi, C. A.; Chiorbelli, C.; Indelli, M. T.; Rampi, M. A. *Coord. Chem. Rev.* **1990**, *97*, 299.
(17) Bignozzi, C. A.; Bortolini, O.; Chiorbelli, C.; Indelli, M. T.; Rampi, M. A.; Scandola, F. *Inorg. Chem.* **1992**, *31*, 172.
(18) Otsuka, T.; Kaizu, Y. *Chem. Lett.* **1997**, 79.
(19) Oetliker, U. *MEASURE* Software for Laboratory Instrument Control and Data Acquisition; Geneva, 1998.
(20) Felix, F.; Ferguson, J.; Gudel, H. U.; Ludi, A. *J. Am. Chem. Soc.* **1980**, *102*, 4096.
(21) Demas, J. N.; Crosby, G. A. *J. Am. Chem. Soc.* **1971**, *93*, 2841.
(22) Schönherr, T.; Spanier, J.; Schmidtke, H.-H. *J. Phys. Chem.* **1989**, *93*, 5969.
(23) Harrigan, R. W.; Hager, G. D.; Crosby, G. A. *Chem. Phys. Lett.* **1973**, *21*, 487.
(24) Krausz, E.; Ferguson, J. *Progr. Inorg. Chem.* **1989**, *37*, 293.
(25) Lacky, D. E.; Pankuch, B. J.; Crosby, G.A. *J. Phys. Chem.* **1980**, *84*, 2068.
(26) Henderson, B.; Imbusch, G. F. *Optical Spectroscopy of Inorganic Solids*; Clarendon Press: Oxford, 1989; p 445 ff.
(27) Förster, Th. *Ann. Phys.* **1948**, *2*, 55.
(28) Dexter, D. L. *J. Chem. Phys.* **1953**, *21*, 836.
(29) von Arx, M. E.; Oetliker, U.; Hauser, A. 1999. In preparation.
(30) (a) Blasse, G.; Grabmaier, B. C. *Luminescent Materials*; Springer-Verlag: Berlin, 1994. (b) Blasse, G. *Recl. Trav. Chim. Pays-Bas* **1986**, *105*, 143.
(31) Maruszewski, K.; Kincaid, J. C. *Inorg. Chem.* **1995**, *34*, 2002.
(32) Sykora, M.; Kincaid, J. R.; Dutta, P. K.; Castagnola, N. B. *J. Phys. Chem. B* **1999**, *103*, 309.